Biosensors and Bioelectronics 24 (2009) 2864–2870

Contents lists available at ScienceDirect

Biosensors and Bioelectronics

journal homepage: www.elsevier.com/locate/bios

Structural properties and sensing performance of high-k Nd_2TiO_5 thin layer-based electrolyte–insulator–semiconductor for pH detection and urea biosensing

Tung-Ming Pan[a,*], Jian-Chi Lin[a], Min-Hsien Wu[b], Chao-Sung Lai[a]

[a] Department of Electronics Engineering, Chang Gung University, Taoyuan 333, Taiwan, ROC
[b] Graduate Institute of Biochemical and Biomedical Engineering, Chang Gung University, Taoyuan 333, Taiwan, ROC

ARTICLE INFO

Article history:
Received 19 November 2008
Received in revised form 13 February 2009
Accepted 17 February 2009
Available online 27 February 2009

Keywords:
Electrolyte–insulator–semiconductor (EIS)
pH
Nd_2TiO_5
Sensors
Urea

ABSTRACT

For high sensitive pH sensing, an electrolyte–insulator–semiconductor (EIS) device with Nd_2TiO_5 thin layers fabricated on Si substrates by means of reactive sputtering and the subsequent post-deposition annealing (PDA) treatment was proposed. In this work, the effect of thermal annealing (600, 700, 800, and 900 °C) on the structural characteristics of Nd_2TiO_5 thin layer was investigated by X-ray diffraction, X-ray photoelectron spectroscopy, and atomic force microscopy. The observed structural properties were then correlated with the resulting pH sensing performances. For enzymatic field-effect-transistors-based urea biosensing, a hybrid configuration of the proposed Nd_2TiO_5 thin layer with urease-immobilized alginate film attached was established. Within the experimental conditions investigated, the EIS device with the Nd_2TiO_5 thin layer annealed at 800 °C exhibited a higher pH detection sensitivity of 57.2 mV/pH, a lower hysteresis voltage of 2.33 mV, and a lower drift rate of 1.80 mV/h compared to those at other annealing temperatures. These results are attributed to the formation of a thinner low-k interfacial layer at the oxide/Si interface and the higher surface roughness occurred at this annealing temperature. Furthermore, the presented urea biosensor was also proved to be able to detect urea with good linearity (R^2 = 0.99) and reasonable sensitivity of 9.52 mV/mM in the urea concentration range of 3–40 mM. As a whole, the present work has provided some fundamental data for the use of Nd_2TiO_5 thin layer for EIS-based pH detection and the extended application for biosensing.

1. Introduction

The ion-sensitive field-effect transistors (ISFETs), first demonstrated by Bergveld (1970), are solid-state electronic devices for chemical sensing of ion concentrations in solution (e.g. hydrogen ions for pH measurement). With the recent advance in microelectronic technology, ISFET-based sensing mechanism plays an important role in the development of microsensors mainly due to the features of low cost, ease of miniaturization, as well as low output impedance (Bergveld, 2003). Borrowing from the well-established ISFET sensing mechanism, pH-ISFET-based biosensors has been actively proposed for various biosensing purposes such as glucose (Luo et al., 2004), lactate (Kharitonov et al., 2001), creatinine (Premanode and Toumazou, 2007), urea (Boubriak et al., 1995) or DNA (Bandiera et al., 2007). The fundamental configuration of biosensing of these kinds is based on the conjugation of a pH sensitive electrode with a biological recognition layer normally containing enzymes specific to the detection target. The rationale behind is that the immobilized enzyme molecules specifically react with the target of detection and leads to the change of pH in solution. The alteration of pH level in the tested solution, closely correlating with the concentration of detection target, is in turn quantified by the pH-ISFET-based sensing mechanism. The biosensing device based on this arrangement is also referred to as enzymatic field-effect transistors (EnFETs) biosensor.

The sensing characteristics of EnFET-based biosensing are, to a great extent, dependent on the performance of the ISFET-based pH sensing mechanism. ISFET is typically built by replacing the metallic gate in a metal-oxide-semiconductor field-effect transistor (MOSFET) with a thin membrane. Reports in literature have demonstrated that the material, composition as well as the fabrication process of the thin membrane in an ISFET structure have important bearings on the resulting ISFET-based sensing performances (Matsuo et al., 1979; Fog and Buck, 1984; Bergveld, 2003). For example, silicon nitride (Si_3N_4) sensing membrane is the most popular material of choice for pH-ISFET mainly due to the ease of fabrication, high compatibility for complementary metal-oxide-semiconductor (CMOS) integration (Chen et al., 1993). However, pH-ISFET devices based on Si_3N_4 sensing membrane normally show unstable properties on threshold voltage stemming from the conversion of silicon nitride film to a hydrated silicon dioxide (SiO_2)

* Corresponding author. Tel.: +886 3 211 8800x3349; fax: +886 3 211 8507.
E-mail address: tmpan@mail.cgu.edu.tw (T.-M. Pan).

0956-5663/$ – see front matter © 2009 Elsevier B.V. All rights reserved.
doi:10.1016/j.bios.2009.02.018

or an oxynitride layer during the contact with an aqueous solution (Jamasb et al., 1998a,b). In order to solve this problem, several high dielectric constant (high-*k*) materials, including Al_2O_3, Ta_2O_5, ZrO_2, HfO_2, Y_2O_3, Gd_2O_3 and Pr_2O_3 were recently proposed as a pH sensing membrane borrowing from their good sensing performance and highly thermal stability, as demonstrated in the literature (Bousse et al., 1990; Kwon et al., 1996; Yoshida et al., 2004; Lai et al., 2006; Pan and Liao, 2007, 2008; Chang et al., 2006). Nevertheless, the poor interface existing in between the metal oxide and Si substrate (Wilk et al., 2001) remains a technical hurdle to overcome.

Conversely, TiO_2 film combining with lanthanide oxide has been proved to be stable against moisture (Mane et al., 2005), providing a thin interfacial layer (Jeon and Hwang, 2002). For example, van Dover (van Dover, 1999) has demonstrated that an interface formed by incorporating TiO_2 or Ti into lanthanide oxide films can achieve a high-*k* dielectric material existing above the interface with excellent electrical properties in terms of a large dielectric constant, a high breakdown voltage, and a low leakage current. On the other hand, apart from those previously mentioned high-*k* materials, it was also reported recently that the rare-earth (RE) oxides are potential materials for gate dielectric due to their reasonably high relative permittivity, large conduction band offset and good thermal stability with Si substrate (Nigro et al., 2004; Fanciulli and Scarel, 2007). Nd_2O_3, a typical RE oxide, is an attractive material to substitute the previous high-*k* materials in the CMOS devices because of its excellent electrical properties including a thin capacitance equivalent thickness, a high electric breakdown field, a low interface trap density, a small hysteresis and frequency dispersion, which has been demonstrated in our previous study (Pan et al., 2006).

Taken together, high-*k* Nd_2TiO_5 thin layer deposited on Si substrate is proposed with the hope of achieving an ideal ISFET-based sensing performance. To the best of our knowledge, the structural properties and sensing performance of Nd_2TiO_5 thin layer have not yet been explored. In this work, the nature of Nd_2TiO_5 thin layer formed on silicon substrate by means of physical vapor deposition (PVD) technique and the subsequent post-deposition annealing (PDA) process with varied temperature of 600 °C, 700 °C, 800 °C and 900 °C were investigated. Briefly, the growth directions and the crystallinity of the Nd_2TiO_5 films after annealing at different temperatures were analyzed using X-ray diffraction (XRD). Also, the chemical structure and surface morphologies of Nd_2TiO_5 films were examined by X-ray photoelectron spectroscopy (XPS) and atomic force microscopy (AFM), respectively. Moreover, the observed structural properties of the Nd_2TiO_5 films investigated were then correlated with the resulting pH sensing performances including detection sensitivity, hysteresis and signal drifting. Furthermore, as a demonstration case for EnFET-based urea biosensing, urease-immobilized film was prepared by the entrapment of enzyme molecules in alginate hydrogel. The thin film was then physically attached on the Nd_2TiO_5 sensing membrane of PDA at 800 °C. The working principle is based on the chemical reaction of urea with urease to cause pH alteration in the tested solution, and in turn resulting in detection response in the pH-EIS mechanism. By this sensing scheme, the urea in solution can be quantified indirectly. In this research, the hybrid configuration of the proposed Nd_2TiO_5 sensing membrane with urease-immobilized film attached was proved to be able to detect urea with good linearity ($R^2 = 0.99$) and reasonable sensitivity of 9.52 mV/mM in the urea concentration range of 3–40 mM, which is sufficient for general clinical examination of blood urea. As a whole, the present work has provided some fundamental data for the use of Nd_2TiO_5 sensing membrane for EIS-based pH detection and the extended application for biosensing.

2. Materials and methods

2.1. Fabrication of EIS pH sensor

Electrolyte–insulator–semiconductor (EIS) capacitors with Nd_2TiO_5 sensing membranes were fabricated on 4-in p-type (1 0 0) Si wafers with a resistivity of 5–10 Ω cm. Prior to the deposition of Nd_2TiO_5 film, the wafers were cleaned by a standard Radio Corporation of America (RCA) process and then dipped in 1% hydrofluoric acid to remove native oxide from the surface. A ~20 nm Nd_2O_3 film was deposited on the Si substrate through reactive sputtering from a neodymium target in diluted O_2. Then, a ~15 nm Ti film was deposited on the Nd_2O_3 by means of sputtering from a titanium target. Samples were annealed at various temperatures in O_2 ambient for 30 s by rapid thermal annealing (RTA) to form Nd_2TiO_5 sensing film. A 4000-Å-thick Al film was deposited as the backside contact of the Si wafer. The sensing membrane size was defined through photolithographic processing under a photosensitive epoxy (SU8-2005, MicroChem Inc.) that acts as an antiacid polymer. EIS devices were then fabricated on the copper lines of a printed circuit board by using a silver gel to form conductive lines. A hand-made epoxy package was used to encapsulate the EIS structure and the copper line.

2.2. Evaluation of the structural properties and pH sensing performance

After fabrication processes, the structure and composition of the Nd_2TiO_5 sensing membranes annealed at different temperatures were then investigated using XRD and XPS. The surface morphologies of Nd_2TiO_5 films were examined by AFM. On the other hand, to evaluate the resulting EIS-based pH sensing performance of the above Nd_2TiO_5 membranes, the pH detection of standard buffer solution (Merck Inc., USA) with pH level ranging from pH 2 to pH 12 was carried out. Briefly, to saturate the ionic properties of the tested sensing membranes, all EIS devices fabricated were firstly immersed in reversed osmosis (R.O.) water for 12 h prior to the measurements. The capacitance–voltage (*C*–*V*) curves for the standard buffer solutions with varied pH levels were then measured through Ag/AgCl reference electrode by Hewlett-Packard (HP) 4284A LCR meter with an ac signal frequency of 100 Hz. All of the experimental setups were held in a dark condition to possibly prevent the interference caused by the ambient light and noise. The detection sensitivity of the Nd_2TiO_5 sensing membranes investigated in this research were then evaluated by the *C*–*V* curves.

2.3. Urea biosensing

As a demonstration case of EnFET-based biosensing, urea detection was performed by configuring a hybrid structure encompassing the aforementioned EIS-based pH sensor with a thin layer (1 mm) of urease-immobilized alginate hydrogel attaching on the top of Nd_2TiO_5 membrane. Shortly, urease (from Jack Beans, ~100 U/mg: unless otherwise stated all chemicals were purchased from Sigma, Taiwan) solution prepared in phosphate buffered saline (PBS) was thoroughly mixed with alginate suspension to form a urease/alginate suspension with the resulting concentrations of 0.1 mg/L and 1.5% (w/v), respectively. The suspension was then loaded onto a clean glass slide and followed by covering with another glass slide with a 1 mm thick spacer in between, allowing the definition of the thickness of alginate thin layer. In the following gelatinization process, the above sandwich like structure was then submerged in 102 mM calcium chloride solution for about 10 min. The prepared thin enzyme-containing alginate gel was subsequently shaped according to the zone of Nd_2TiO_5 sensing membrane using a borer and followed by attaching on the surface of

the sensing membrane. To test the feasibility of using the proposed sensor for urea detection, the prepared sensor was sequentially immersed in urea solutions with varied concentrations of 3, 10, 20, 30 and 40 mM with measurement time of 5 min for each condition. Also, there was a clean procedure by rinsing the used sensor with R.O. water between two measurements. In this study, urea standard solutions with various concentrations were made using PBS to solve urea powder and the resulting pH levels of each cases were examined to be equal by a commercial pH meter.

3. Results and discussion

3.1. Structural properties

It is well known fact that annealing treatments under oxygen ambient can improve the optical and structural properties (Singh et al., 2003) of the RE metal oxides, due to the reduction of defect density and the optimization of oxide stoichiometry. Besides, it has also been reported that the annealing processes may induce strong interfacial reactions, leading to the formation of silicate layers (Mikhelashvili et al., 2004). Our previous studies (Pan et al., 2006) have revealed that the thermal annealing conditions have significant effect on the properties of the interfacial layer in between the deposited oxides and Si substrate underneath and also on other structural characteristics. These could accordingly connect to the performances of the resulting ISFET-based sensing. To find out the impact of thermal annealing conditions on the structural properties of deposited Nd_2TiO_5 thin layer in EIS structure, the following analyses were carried out (Fig. 1). To explore the effect of the PDA treatment at different temperatures (600 °C, 700 °C, 800 °C and 900 °C) on the crystalline nature of the Nd_2TiO_5 sensing film, XRD measurements was conducted. Results (Fig. 1) revealed that the film formed at the PDA of 600 °C and 700 °C showed weaker peak (2 3 0) intensity compared with the other higher PDA cases, indicative of an amorphous Nd_2TiO_5 structure (orthorhombic phase). For higher PDA cases, stronger peak (2 3 0) intensities were observed in both cases while two peaks with lower intensities at (4 3 1) and (0 3 1) were found in the 800 °C and 900 °C cases, respectively.

Besides, to further investigate the influence of the PDA treatment on the compositional properties of the deposited Nd_2TiO_5 thin layer, XPS analysis was carried out. Fig. 2(A) showed the Nd 3d XPS spectra of the Nd_2TiO_5/Si interface annealed at various temperatures as aforementioned. The position of Nd 3d peak occurred at the binding energy of 984.5 eV indicates the formation of Nd_2TiO_5. It can be noticed from Fig. 2(A) that the formation of Nd_2TiO_5 thin layers was observed when the annealing temperature is below 800 °C. Conversely, the Nd 3 peak position of the film fabricated at the PDA of 900 °C slightly shifted by about 0.5 eV compared with the Nd_2TiO_5 reference peak position of 984.5 eV, indicating the formation of Nd-silicate (Pan et al., 2006). This can be explained by the fact that the Si atoms diffused toward the interfacial area during thermal annealing and consequently resulted in the interaction of Nd and Si atoms. Moreover, the Fig. 2(B) showed the XPS binding energy of Ti 2p peaks for the Nd_2TiO_5 thin layers annealed at different temperatures. In the Ti 2p spectra, the Ti 2p splitting position (Ti $2p_{1/2}$ and Ti $2p_{3/2}$ at 465.4 and 459.5 eV, respectively) of Nd_2TiO_5 film is shifted to a higher binding energy compared to the TiO_2 reference peak (Ti $2p_{1/2}$ and Ti $2p_{3/2}$ at 464.3 and 458.7 eV, respectively) (Schroeder et al., 2005). It is found that the Nd_2TiO_5 film performed at 600 °C shifts the Ti 2p peak position to a higher binding energy by 0.1 eV

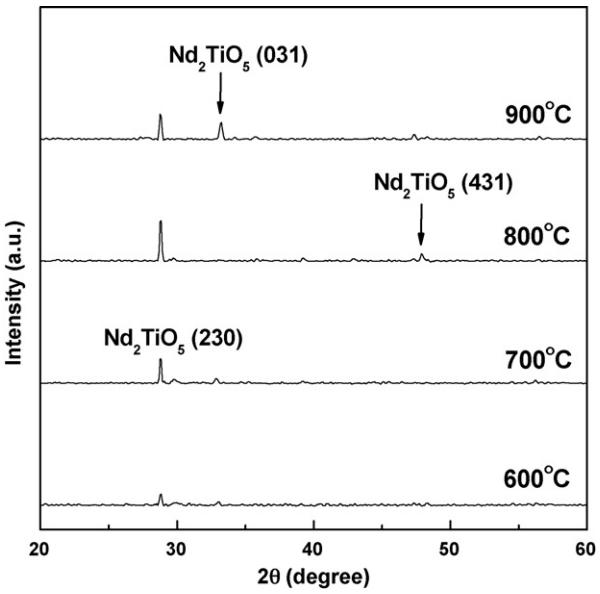

Fig. 1. XRD patterns of Nd_2TiO_5 films annealed at various temperatures.

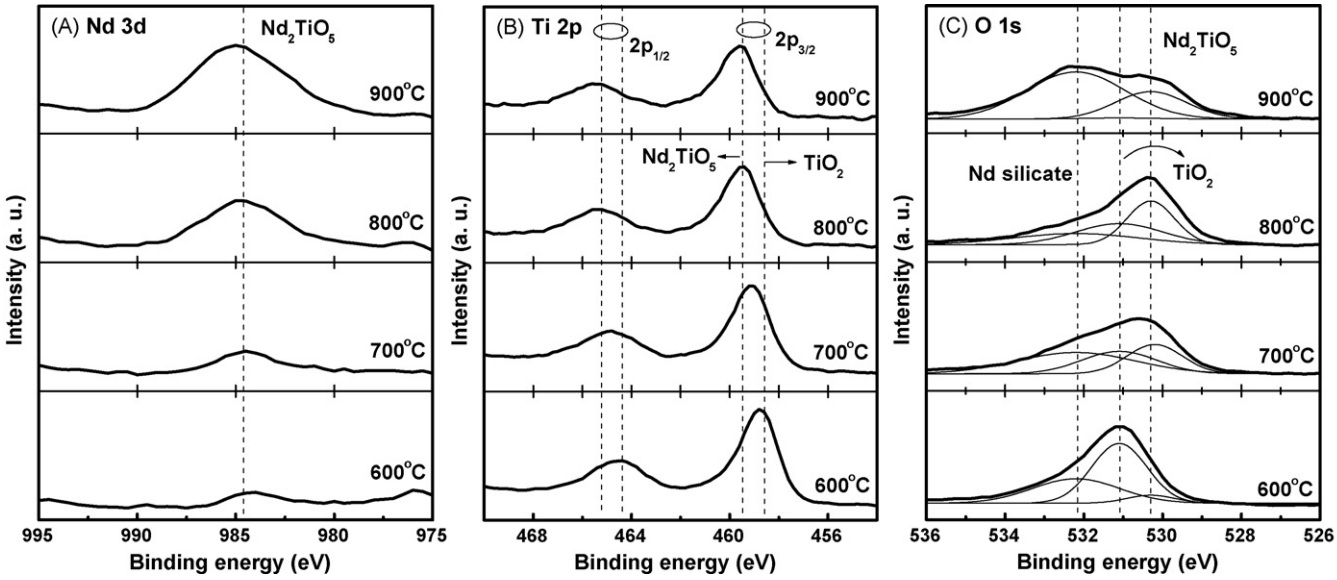

Fig. 2. XPS spectra of (A) Nd 3d, (B) Ti 2p, and (C) O 1s for Nd_2TiO_5 films after RTA at different temperatures.

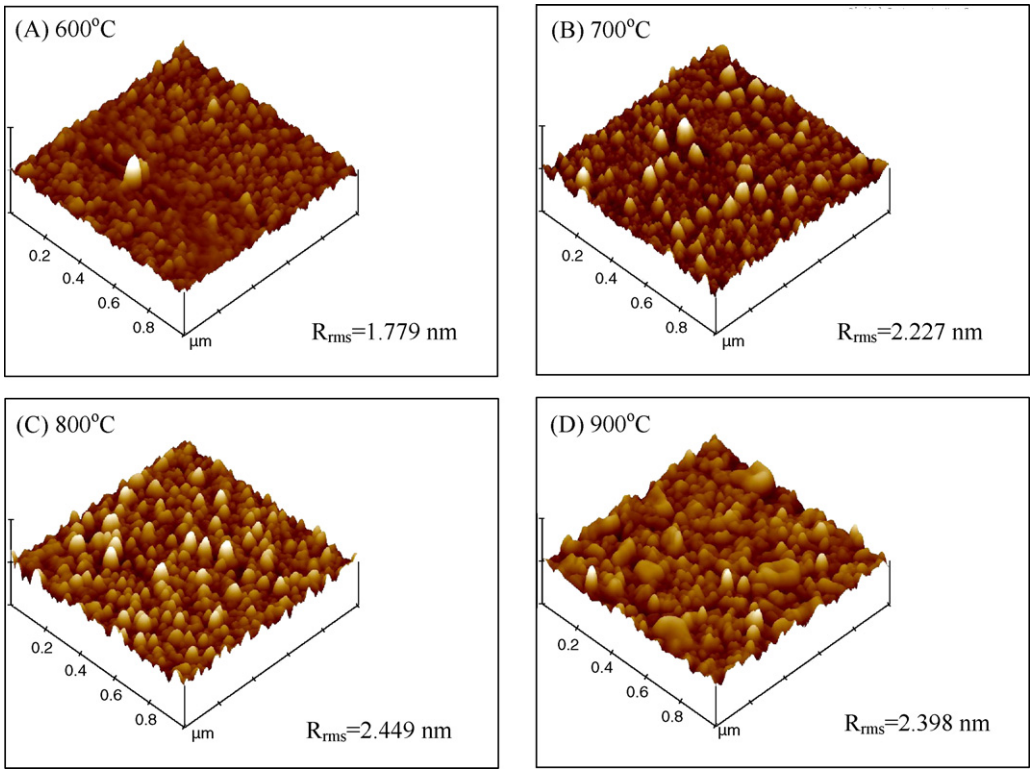

Fig. 3. AFM surface images of Nd_2TiO_5 films after PDA at different temperatures.

compared to TiO_2 peak position, suggesting the badly crystallized Nd_2TiO_5 structure with a higher TiO_2. The chemical shift toward lower binding energy of the Ti 2p peak for the film annealed at 800 °C was smaller by 0.1 eV than Nd_2TiO_5 peak position, probably indicative of the well-crystallized Nd_2TiO_5 structure. However, the shifting of the Ti 2p peak to a higher binding energy for the sample after RTA at 900 °C is 0.2 eV. This shift is due to the formation of a thicker Nd-silicate layer as aforementioned.

The O 1s spectra for the Nd_2TiO_5 films after PDA treatment are shown in Fig. 2(C) with their appropriate peak curve-fitting lines corresponding to chemical states. In three sets of spectra, each fitting peak is assumed to follow the general shape of the Gaussian function. The low-energy state, peak located at 530.3 eV, is attributed to O in Nd_2TiO_5. The intermediate-energy state, peak located at 531.1 eV, is assigned to O in TiO_2 (Schroeder et al., 2005). The high-energy state, peak located at 532.2 eV, is attributed to interfacial O atoms in nonstoichiometric silicate ($NdSi_xO_y$) (Pan et al., 2006). The sample annealed at 600 °C appears to be composed mainly of Nd-silicate and TiO_2. The O 1s peak intensity corresponding to TiO_2 decreases upon increasing the RTA temperature, while the O 1s peak intensity corresponding to Nd_2TiO_5 increases upon increasing the RTA temperature, but decreased suddenly at 900 °C. This finding suggests that the neodymium moving from the Nd_2TiO_5 film was mostly consumed by the larger formation of Nd-silicate layer.

Apart from the structural and compositional properties mentioned previously, it has also been demonstrated that the surface roughness of dielectric/electrode interface can significantly influence the sensitivity of ISFET-based pH detection (Lai et al., 2006). In order to understand the surface nature of Nd_2TiO_5 thin layers annealed at various temperatures, AFM analysis was conducted. It can be clearly seen from Fig. 3 that a bimodal response to annealing temperature was observed, where surface roughness was greatest at the temperature of 800 °C (root mean square roughness (R_{rms}): 2.449 nm) and further increase or decrease of annealing temperature was found to reduce surface roughness. This phenomenon may be explained by the fact that the crystallization and/or grain growth took place on the surface of deposited oxide when the annealing temperature increased from 600 °C to 800 °C, contributing to a rougher surface. However, further increase of annealing temperature (e.g. 900 °C in this study), the most of Nd atoms removed from the deposited thin layer could migrate to the interface and therefore increase the formation of an amorphous silicate layer. This may lead to a less rough surface as seen in Fig. 3(D).

3.2. pH sensing performance

In pH-EIS sensing, the change of pH level normally causes the flat-band voltage shift of the *C–V* curves. This result is mainly due to the ionization of the surface hydroxyl groups by hydrogen ions or hydroxyl ions (Fung et al., 1986). In order to evaluate the sensing performance of the Nd_2TiO_5 thin layer annealed at different temperatures, the *C–V* curves of these cases studied at the pH levels ranging from pH 2 to pH 12 were experimentally investigated. In this study, the reference voltages were determined from the obtained *C–V* curves at the normalized capacitance of 0.2 (Fig. 4(A): inset). Results (Fig. 4(A)) revealed that the reference voltage for Nd_2TiO_5 sensing films shifted accordingly with the change of pH level ranging from pH 2 to pH 12. This finding is mainly due to the alteration of surface potential caused by the change in the number of hydrogen ion on the Nd_2TiO_5 sensing layer. In terms of pH detection sensitivity of the Nd_2TiO_5 sensing layers fabricated under different annealing temperatures, results (Fig. 4(B)) showed that the EIS device with a Nd_2TiO_5 thin layer annealed at 800 °C exhibited a better detection sensitivity of 57.2 mV/pH, compared with that of 32.21 mV/pH, 52.5 mV/pH and 50.1 mV/pH for the sensing layers prepared at 600 °C, 700 °C and 900 °C, respectively. This outcome could be attributed to the higher surface roughness of Nd_2TiO_5 thin layer and thinner Nd-silicate layer as discussed previously in Figs. 2 and 3. It is generally accepted that ISFET-based

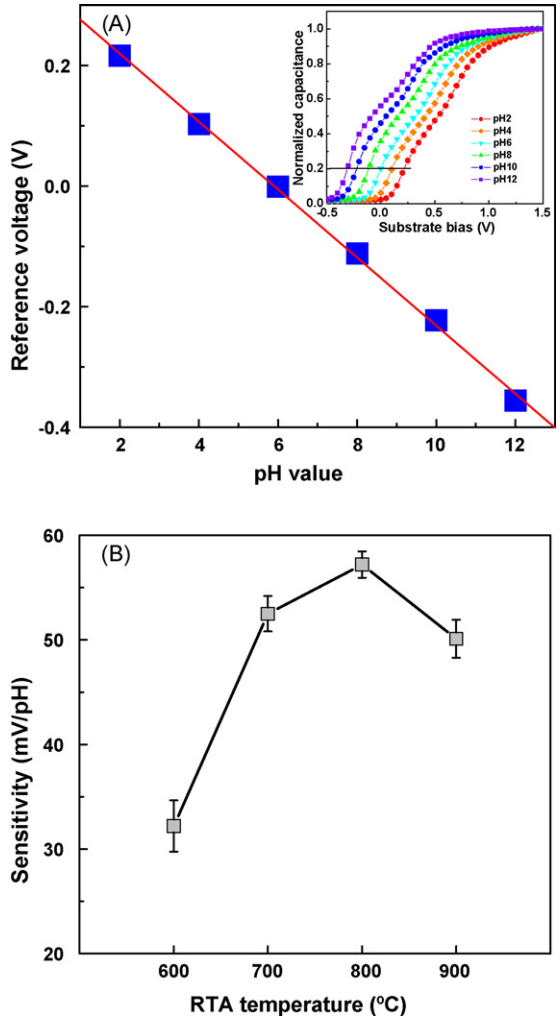

Fig. 4. (A) Reference voltage of Nd_2TiO_5 sensing membrane annealed at 800 °C as a function of pH at room temperature. The inset shows the *C–V* curves response of EIS device using a Nd_2TiO_5 dielectric after PDA at 800 °C when inserted into solutions with pH values from 2 to 12. (B) pH sensitivity of EIS devices using Nd_2TiO_5 sensing membranes as a function of RTA temperatures. Data were presented as mean ± S.D. from six independent experiments.

pH sensing mechanism can be well described by the site-binding model (Siu and Cobbold, 1979). According to the model, with the higher surface roughness, the total number of surface site per unit area will increase accordingly, which therefore contributes to higher detection sensitivity. This phenomenon has also been demonstrated in our previous studies (Pan and Liao, 2008). On the other hand, within the experimental conditions investigated, the lowest detection sensitivity occurred at the case of 600 °C (Fig. 4(B)) and this is probably due to the formation of smoother surface and a badly crystallized structure as observed in Figs. 2 and 3. Besides, the relative standard deviations (R.S.D.) of the detections in such evaluation were calculated to be 7.60%, 3.24%, 2.19%, and 3.61% ($n = 6$) for the EIS devices with Nd_2TiO_5 thin layers fabricated at the PDA of 600 °C, 700 °C, 800 °C, and 900 °C, respectively. This adequately meets the requirement of within 10% of R.S.D. for general sensing devices.

Apart from the detection sensitivity, hysteresis phenomenon is one of the important performances of a sensing device. In EIS-based pH sensing, the hysteresis phenomenon could be due to the defects of a dielectric film, resulting in the formation of porous structures. The interior sites of these porous detects could react with the ions existing in the tested solution and thus causes hysteresis response. Another possible cause is the interaction of ions in the solution with the responding sites along the boundaries of grains on an insulator film (Bousse et al., 1990). In this work, the hysteresis of pH sensing of the proposed EIS devices with varied Nd_2TiO_5 thin layers studied were evaluated directly by immersing the prepared sensors in each pH standard solution for up to 5 min in the set cycle of pH 7 → 4 → 7 → 10 → 7 and 7 → 10 → 7 → 4 → 7. The hysteresis voltage discussed here is defined as the gate voltage difference between the initial and terminal voltages measured in the above cycle. Fig. 5(A) and (B) showed the profiles of the evaluation in the set cycle of pH 7 → 4 → 7 → 10 → 7 and 7 → 10 → 7 → 4 → 7, respectively. It can be found from the results that the hysteresis voltage of EIS device with the Nd_2TiO_5 sensing film prepared at 800 °C showed the lowest value of 2.53 mV and 4.57 mV for the pH loop of pH 7 → 4→ 7→ 10 → 7 and 7 → 10 → 7 → 4 → 7, respectively within the experimental conditions investigated. This could be due to the formation of a thinner Nd-silicate interfacial layer and a rougher surface, accordingly leading to the formation of smaller number of interior sites occurred in the 800 °C case. Conversely, the EIS device with Nd_2TiO_5 sensing film annealed at 600 °C exhibited the highest hysteresis voltage of 10.2 mV and 35.8 mV in the pH loops of pH 7 → 4→ 7 → 10 →7 and 7 → 10 → 7 → 4→ 7, respectively. This observation may be resulted from the formation of a badly crystallized Nd_2TiO_5 structure with high content of TiO_2. Besides, regarding the reproducibility of measurements, the R.S.D. of the hysteresis evaluation in the set pH loop of pH 7 → 4→ 7→ 10 → 7 were 7.26%, 5.14%, 4.05%, and 4.42% ($n = 6$) for the Nd_2TiO_5-based EIS devices annealed at 600 °C, 700 °C, 800 °C, and 900 °C, respectively. Similarly, it was 7.43%, 5.07%, 4.11%, and 4.38% ($n = 6$) for the 600 °C, 700 °C, 800 °C, and 900 °C cases, respectively in the set pH cycle of pH 7 → 10 → 7 → 4 → 7. All these results again demonstrated the reasonable reproducibility of detections by the proposed Nd_2TiO_5-based EIS devices. Particularly, Nd_2TiO_5-based EIS devices annealed 800 °C exhibited the optimum reproducibility of detection within the experimental conditions explored.

Regarding to the signal drifting issue, the drift rate of pH-ISFET is described using a hopping and/or trap-limited transport mechanism, also known as dispersive transport (Scher and Montroll, 1975; Pfister and Scher, 1977), to evaluate the hydration rate of the insulator. The phenomena of dispersive transport can be found in a broad class of disordered materials. In an amorphous material, for example, dispersive transport may arise from hopping motion through localized states (hopping transport), trap-limited transport in the presence of traps possessing an exponential energy distribution (multiple-trap transport), or a combination of the aforementioned transport mechanisms (trap-controlled hopping transport) (Jamasb et al., 1998a,b). Dispersive transport causes a decay in the density of sites/traps occupied by the species going through transport (Kakalios et al., 1987). The hypothesis that hydration of the gate dielectric is controlled by a dispersive transport mechanism is sustained by the presence of buried surface sites and/or the presence of traps (specifically electrically active silicon dangling bonds). The variations in the chemical composition of the insulator surface leads to the change in number of surface site with time, thus causing a monotonic temporal increase in the threshold voltage. In this study, the drift rate of the Nd_2TiO_5 sensing membrane after different PDA treatments was evaluated after submerging the devices in a pH 7 standard solution for 12 h. Fig. 5(C) showed the drift profiles of the EIS devices with sensing films annealed at various different temperatures. It can be clearly found from Fig. 5(C) that the EIS device with a Nd_2TiO_5 sensing film annealed at 800 °C exhibited optimum stability (1.80 mV/h), whereas the 600 °C case showed the worst stability with the highest drift rate of 7.40 mV/h. The optimum stability of detection observed in the 800 °C case in this investigation may be resulted from the formation of a thinner silicate layer at the oxide/Si interface. However, a higher drift rate in the case of 600 °C

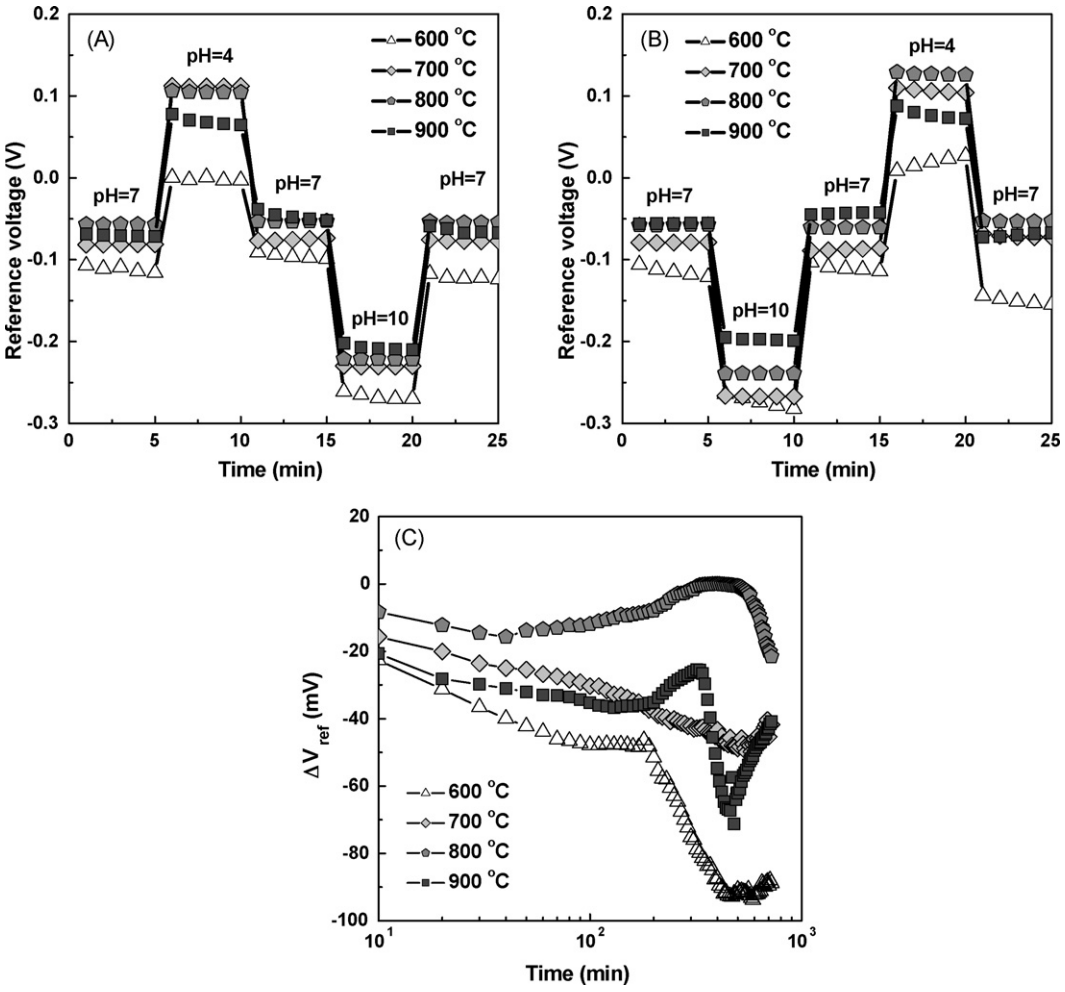

Fig. 5. Hysteresis voltage of EIS devices using Nd_2TiO_5 sensing membranes after RTA treatment during the pH loops (A) 7 → 4 → 7 → 10 → 7 and (B) 7 → 10 → 7 → 4 → 7. (C) Drift rate of EIS capacitors with Nd_2TiO_5 sensing membranes after RTA treatment as a function of times in the pH 7 solution.

was considered to be caused by the less rough surface and a badly crystallized structure as investigated in the previous AFM and XRD spectra, respectively.

3.3. Demonstration case for urea biosensing

Urea ($(NH_2)_2CO$) is basically an organic compound of carbon, nitrogen, oxygen and hydrogen. The excretion of nitrogen waste originating from protein and amino acid catabolism produces some organisms. In aquatic organisms the most common form of nitrogen waste is ammonia, while land-dwelling organisms convert the toxic ammonia to either urea or uric acid (Nelson and Cox, 2004). The normal level of urea in serum is 3–7 mM (15–40 mg/dl). In patients suffering from the renal analysis is of considerable importance in agro-food chemistry and environmental monitoring. As a demonstration case of EnFET-based biosensing, urea detection was performed in this study. The principle of sensing is based on the detection of pH alteration caused by the specific enzyme-substrate (urease-urea) reaction as shown below.

$$NH_2CONH_2 + 3H_2O \xrightarrow{\text{urease}} 2NH_4^+ + OH^- + HCO_3^-$$

For the biosensing of this kind, the strategy for immobilization of bio-recognition element on a transducer has important bearing on the subsequent sensing performances and reliability of a biosensor (Gutierrez et al., 2007; Barhoumi et al., 2006). In this work, a urea biosensor with a hybrid structure of urease-containing alginate film/Nd_2TiO_5 membrane/Si-sub EIS was constructed. Instead of enzyme immobilization by chemical covalent bonding approach, gel entrapment method was adopted to immobilize the enzyme molecules onto Nd_2TiO_5 sensing membrane in this case, provid-

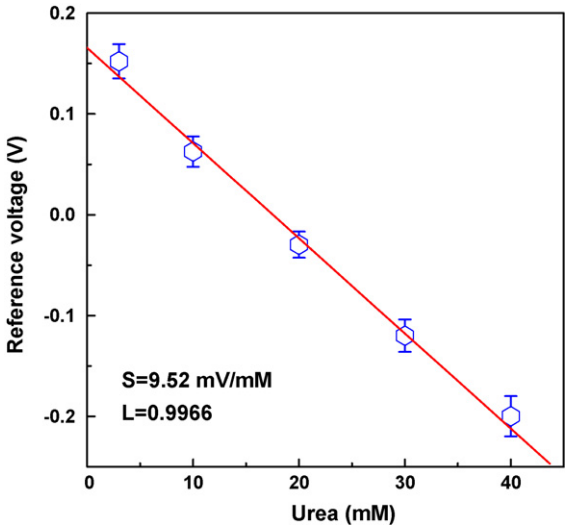

Fig. 6. Reference voltage of a EIS device having Nd_2TiO_5 sensing film annealed at 800 °C as a function of urea concentration. Data are presented as mean ± S.D. from at least six independent experiments.

ing a relatively milder condition to possibly minimize the loss of enzyme activity during immobilization process. Besides, the other feature of the design is that the prepared enzyme/alginate thin film is easy to prepare and is able to reversely attach on the surface of Nd_2TiO_5 membrane. Starodub et al. (1999) have also suggested that alginate hydrogel is a material of choice for creating replaceable enzymatic membranes deposited on a sensor's surface. This characteristic potentially makes disposable urea biosensor possible by simply replacing the enzyme/hydrogel film when every time use. To evaluate the feasibility for biosensing, the calibration curve of urea detection was established in Fig. 6. It is found that the presented device was able to detect urea with good linearity ($R^2 = 0.99$) and reasonable sensitivity of 9.52 mV/mM in the urea concentration range of 3 to 40 mM, which is sufficient for general clinical examination of blood urea.

4. Conclusion

In this study, an EIS device with a high-k Nd_2TiO_5 sensing membrane deposited on silicon substrate through reactive sputtering was proposed for high sensitive pH sensing. The physical properties of Nd_2TiO_5 structure in EIS device were investigated by means of XRD, XPS, and AFM analysis. It was found that, within the experimental conditions explored, the Nd_2TiO_5 EIS device fabricated at the PDA of 800 °C exhibited an optimum pH sensing performance including a higher sensitivity of 57.2 mV/pH, a smaller hysteresis voltage of 2.33 mV and a lower drift rate of 1.80 mV/h. This improvement is attributed to the suppression of the lower-k interfacial layer at the Nd_2TiO_5/Si interface and the higher surface roughness occurred at this condition. Borrowing from the good pH sensing performance of EIS device with a high-k Nd_2TiO_5 sensing membrane, an EnFET-based urea biosensing was proved to be able to detect urea with good linearity ($R^2 = 0.99$) and reasonable sensitivity of 9.52 mV/mM in the urea concentration range of 3–40 mM, which is sufficient for general clinical examination of blood urea. As a whole, a high-k Nd_2TiO_5 sensing membrane was first time demonstrated for high sensitive pH-EIS and was also proved promising for the extended application on biosensing.

Acknowledgment

This work was supported by the National Science Council, Taiwan, Republic of China, under contract no. NSC-97-2221-E-182-050-MY3.

References

Bandiera, L., Cellere, G., Cagnin, S., De Toni, A., Zanoni, E., Lanfranchi, G., Lorenzelli, L., 2007. Biosens. Bioelectron. 22 (9–10), 2108–2114.
Barhoumi, H., Maaref, A., Rammah, M., Martelet, C., Jaffrezic, N., Mousty, C., Vial, S., Forano, C., 2006. Mater. Sci. Eng. C 26 (2–3), 328–333.
Bergveld, P., 1970. IEEE Trans. Biomed. Eng. 17 (1), 70–71.
Bergveld, P., 2003. Sens. Actuators B 88 (1), 1–20.
Boubriak, O.A., Soldatkin, A.P., Starodub, N.F., Sandrovsky, A.K., Elskaya, A.K., 1995. Sens. Actuators B 27 (1–3), 429–431.
Bousse, L., van der Vlekkert, H.H., de Rooij, N.F., 1990. Sens. Actuators B 2 (2), 103–110.
Chang, L.B., Ko, H.H., Lee, Y.L., Lai, C.S., Wang, C.Y., 2006. J. Electrochem. Soc. 153 (4), G330–G332.
Chen, K.M., Li, G.H., Chen, L.X., Zhu, Y., 1993. Sens. Actuators B 13 (1–3), 209–211.
Fanciulli, M., Scarel, G. (Eds.), 2007. Rare Earth Oxide Thin Film: Growth, Characterization, and Applications. Springer, Berlin.
Fog, A., Buck, R., 1984. Sens. Actuators 5 (2), 137–146.
Fung, C.D., Cheung, P.W., Ko, W.H., 1986. IEEE Trans. Electron. Devices 33 (1), 8–18.
Gutierrez, M., Alegret, S., del Valle, M., 2007. Biosens. Bioelectron. 22 (9-10), 2171–2178.
Jamasb, S., Collins, S.D., Smith, R.L., 1998a. IEEE Trans. Electron. Devices 45 (6), 1239–1245.
Jamasb, S., Collins, S., Smith, R.L., 1998b. Sens. Actuators B 49 (1-2), 146–155.
Jeon, S., Hwang, H., 2002. Appl. Phys. Lett. 81 (25), 4856–4858.
Kakalios, J., Street, R.A., Jackson, W.B., 1987. Phys. Rev. Lett. 59 (9), 1037–1040.
Kharitonov, A.B., Zayats, M.Z., Alfonta, L., Katz, E., Willner, I., 2001. Sens. Actuators B 76 (1–3), 203–210.
Kwon, D.H., Cho, B.W., Kim, C.S., Sohn, B.K., 1996. Sens. Actuators B 34 (1–3), 441–445.
Lai, C.S., Yang, C.M., Lu, T.F., 2006. Electrochem. Solid-State Lett. 9 (3), G90–G92.
Luo, X.L., Xu, J.J., Zhao, W., Chen, H.Y., 2004. Biosens. Bioelectron. 19 (10), 1295–1300.
Mane, A.U., Wenger, Ch., Schroeder, T., Zaumseil, P., Lippert, G., Weidner, G., Mussig, H.J., 2005. J. Electrochem. Soc. 152 (6), C399–G402.
Matsuo, T., Esashi, M., Abe, H., 1979. IEEE Trans. Electron. Devices 26 (11), 1856–1857.
Mikhelashvili, V., Eisenstein, G., Edelman, F., Brener, R., Zakharov, N., Werner, P., 2004. J. Appl. Phys. 95 (2), 613–620.
Nelson, D.L., Cox, M.M., 2004. Lehninger Principles of Biochemistry, fourth ed. W.H. Freeman Custom Publishing.
Nigro, R.L., Toro, R.G., Malandrino, G., Fragala, I.L., Rossi, P., Dapporto, P., 2004. J. Electrochem. Soc. 151 (9), F206–F213.
Pan, T.M., Lee, J.D., Shu, W.H., Chen, T.T., 2006. Appl. Phys. Lett. 89 (23), 232908.
Pan, T.M., Liao, K.M., 2007. Sens. Actuators B 127 (2), 480–485.
Pan, T.M., Liao, K.M., 2008. Sens. Actuators B 133 (1), 97–104.
Pfister, G., Scher, H., 1977. Phys. Rev. B 15 (4), 2062–2083.
Premanode, B., Toumazou, C., 2007. Sens. Actuators B 120 (2), 732–735.
Scher, H., Montroll, E.W., 1975. Phys. Rev. B 12 (6), 2455–2477.
Schroeder, T., Lupina, G., Dabrowski, J., Mane, A., Wenger, Ch., Lippert, G., Mussig, H.J., 2005. Appl. Phys. Lett. 87 (2), 022902.
Singh, M.P., Thakur, C.S., Shalini, K., Bhat, N., Shivashankar, S.A., 2003. Appl. Phys. Lett. 83 (14), 2889–2891.
Siu, W.M., Cobbold, R.S.C., 1979. IEEE Trans. Electron. Devices 26 (11), 1805–1815.
Starodub, N.F., Torbicz, W., Pijanowska, D., Starodub, V.M., Kanjuk, M.I., Dawgul, M., 1999. Sens. Actuators B 58 (1–3), 420–426.
van Dover, R.B., 1999. Appl. Phys. Lett. 74 (20), 3041–3043.
Wilk, G.D., Wallace, R.M., Anthony, J.M., 2001. J. Appl. Phys. 89 (10), 5243–5275.
Yoshida, S., Hara, N., Sugimoto, K., 2004. J. Electrochem. Soc. 151 (3), H53–H58.